DOI:10.1093/jnci/djt164
Advance Access publication July 30, 2013

ARTICLE

Effects of Vascular-Endothelial Protein Tyrosine Phosphatase Inhibition on Breast Cancer Vasculature and Metastatic Progression

Shom Goel, Nisha Gupta, Brian P. Walcott, Matija Snuderl, Cristina T. Kesler, Nathaniel D. Kirkpatrick, Takahiro Heishi, Yuhui Huang, John D. Martin, Eleanor Ager, Rekha Samuel, Shuhan Wang, John Yazbek, Benjamin J. Vakoc, Randall T. Peterson, Timothy P. Padera, Dan G. Duda, Dai Fukumura, Rakesh K. Jain

Manuscript received October 3, 2012; revised May 16, 2013; accepted May 17, 2013.

Correspondence to: Dai Fukumura, MD, PhD, and Rakesh K. Jain, PhD, Edwin L. Steele Laboratory for Tumor Biology, Cox 7, 100 Blossom St, Massachusetts General Hospital, Boston, MA 02114 (e-mail: dai@steele.mgh.harvard.edu and jain@steele.mgh.harvard.edu).

Background The solid tumor microvasculature is characterized by structural and functional abnormality and mediates several deleterious aspects of tumor behavior. Here we determine the role of vascular endothelial protein tyrosine phosphatase (VE-PTP), which deactivates endothelial cell (EC) Tie-2 receptor tyrosine kinase, thereby impairing maturation of tumor vessels.

Methods AKB-9778 is a first-in-class VE-PTP inhibitor. We examined its effects on ECs in vitro and on embryonic angiogenesis in vivo using zebrafish assays. We studied the impact of AKB-9778 therapy on the tumor vasculature, tumor growth, and metastatic progression using orthotopic models of murine mammary carcinoma as well as spontaneous and experimental metastasis models. Finally, we used endothelial nitric oxide synthase (eNOS)–deficient mice to establish the role of eNOS in mediating the effects of VE-PTP inhibition. All statistical tests were two-sided.

Results AKB-9778 induced ligand-independent Tie-2 activation in ECs and impaired embryonic zebrafish angiogenesis. AKB-9778 delayed the early phase of mammary tumor growth by maintaining vascular maturity ($P < .01$, t test); slowed growth of micrometastases ($P < .01$, χ^2 test) by preventing extravasation of tumor cells ($P < 0.01$, Fisher exact test), resulting in a trend toward prolonged survival (27.0 vs 36.5 days; hazard ratio of death = 0.33, 95% confidence interval = 0.11 to 1.03; $P = .05$, Mantel–Cox test); and stabilized established primary tumor blood vessels, enhancing tumor perfusion ($P = .03$ for 4T1 tumor model and 0.05 for E0771 tumor model, by two-sided t tests) and, hence, radiation response ($P < .01$, analysis of variance; n = 7 mice per group). The effects of AKB-9778 on tumor vessels were mediated in part by endothelial nitric oxide synthase activation.

Conclusions Our results demonstrate that pharmacological VE-PTP inhibition can normalize the structure and function of tumor vessels through Tie-2 activation, which delays tumor growth, slows metastatic progression, and enhances response to concomitant cytotoxic treatments.

J Natl Cancer Inst;2013;105:1188–1201

Unlike blood vessels in healthy tissue, the solid tumor microvasculature is dysfunctional and immature. Tumor vessels harbor structural and functional instability, which facilitates several distinct stages of tumor progression, including early sprouting angiogenesis, metastatic cell extravasation into distant organs, and the development of established tumor hypoxia, which fuels metastasis and impairs the efficacy of antitumor therapies (1–9).

The endothelial cell (EC) receptor tyrosine kinase Tie-2/Tek is a critical regulator of vascular maturity. Tie-2 activation by its agonistic ligand angiopoietin 1 (Ang-1) increases perivascular cell (PVC) coverage, tightens EC junctions, reduces permeability, and increases vessel diameter (10–12). Angiopoeitin-2 (Ang-2) antagonizes the effects of Ang-1 in a context-dependent manner (6). Recent studies have shown a deleterious role for Ang-2 in mediating tumor vessel abnormalities and metastasis (13,14), suggesting that Tie-2 deactivation by Ang-2 in part mediates the unstable vessel phenotype seen within tumors. Current strategies targeting the Ang/Tie-2 axis in tumors have focused primarily on direct targeting of the angiopoietins, but such studies have not directly examined complex context-dependent interactions between Ang-1 and Ang-2 or the effects of angiopoietin blockade on Tie-2 activity (15–18). There are currently 10 agents targeting the Ang/Tie-2 axis under investigation in clinical trials (19).

Vascular endothelial protein tyrosine phosphatase (VE-PTP) is an EC-specific receptor tyrosine phosphatase that dephosphorylates and consequently inactivates Tie-2 (20). The role of VE-PTP in

the tumor vasculature is unknown. Recently, AKB-9778 has been developed as a novel, potent, and selective inhibitor of VE-PTP through structural modifications of 1,2,3,4-tetrahydroisoquinolinyl sulfamic acids (21). We hypothesized that pharmacological VE-PTP inhibition would activate Tie-2 signaling in ECs independent of Ang-1/Ang-2 ligands, stabilizing tumor vessels and mitigating the negative consequences of tumor vessel instability (20).

Methods

Cell Lines and Cell Culture

The sources of human umbilical vein endothelial cells (HUVECs), human microvascular endothelial cells (HMVECs), 4T1, and E0771 cells, the derivation of *MMTV-PyVT* tumor cells, and the culture conditions of these cells are described in the Supplementary Materials (available online). In short, ECs were cultured in endothelial growth medium (Lonza, Allendale, NJ), and tumor cells were cultured in Dulbecco's modified Eagle's medium with 10% serum and additional growth supplements as per standard protocols.

Short Hairpin RNA (shRNA) and Lentiviral Delivery

For silencing of Tie-2 in HUVECs, we screened a lentiviral target gene set to *TEK* (synonym: *TIE2*, accessions NM_000459, AB208796, BC035514, and L06139; Thermo Scientific, Logan, UT). Lentiviral particles were generated by cotransfection of pLKO.1-*shTEK*, pVSVG, and pΔVPR into HEK293T cells using the Fugene6 protocol (Roche, Indianapolis, IN). Silencing efficiency of *TEK* in ECs was determined by Western blotting, and clone ID TRCN0000000415 was chosen. Lentiviral particles containing a scrambled shRNA sequence were purchased from Sigma (St Louis, MO). Low passage HUVECs were transduced for 24 hours and then subjected to antibiotic selection with 2 mcg/mL puromycin for 24 to 48 hours.

Animal Use

All animal procedures were performed following the guidelines of Public Health Service Policy on Humane Care of Laboratory Animals and approved by the Institutional Animal Care and Use Committee of the Massachusetts General Hospital, Boston, Massachusetts. Zebrafish and mice were bred and maintained in the MGH Cardiovascular Research Center and in a gnotobiotic animal facility in the Edwin L. Steele Laboratory (suppliers listed in Supplementary Materials, available online), respectively.

Zebrafish Embryonic Angiogenesis Assays

Flk-1:GFP (GFP, green fluorescent protein) transgenic zebrafish were obtained from the MGH Cardiovascular Research Center (Charlestown, MA). Fertilized eggs were incubated in E3 fish water with or without AKB-9778. Embryos were examined under an epifluorescent stereomicroscope at 48 hours postfertilization to manually count the number of intersegmental vessels reaching the dorsal longitudinal anastomotic vessel.

Zebrafish Xenograft Assays

Zebrafish tumor xenografts were established using modifications of a previously published protocol (22) (details in Supplementary Methods, available online). Tumor neovascularization was examined by confocal microscopy; axial sections were obtained through the entire tumor mass, and five sections were analyzed per embryo. Neovascularization was quantified by the ratio of GFP-positive area (ECs) to dsRed-positive area (tumor mass) using ImageJ software (National Institutes of Health, Bethesda, MD).

In Vitro Detection of Nitric Oxide Production in HUVECs Using DAF-2 DA

In vitro detection of EC nitric oxide production was performed through a modified version of previously published protocols (23) using the DAF-2 DA fluorescent indicator. Details are provided in the Supplementary Methods (available online).

Mouse Tumor Models

C57BL6/J, FVB/N, and FVB/N-Tg(*MMTV-PyVT*)634Mul/J mice were originally obtained from Jackson Laboratories (Bar Harbor, ME), and *Nos3*$^{-/-}$ mice were obtained from Dr Paul L. Huang (Massachusetts General Hospital, Boston, MA). Experiments were all performed on female mice aged 6 to 8 weeks. Methods for tumor cell injection are detailed in the Supplementary Materials (available online). The number of animals in each experimental group is detailed in the figure legends.

Drug Treatment of Mice

AKB-9778 dissolved in 5% dextrose was injected at 40 mg/kg subcutaneously every 12 hours, except where otherwise specified. Control vehicle was the same volume of 5% dextrose. Doxorubicin was given at 2.5 mg/kg by intraperitoneal injection every 72 hours.

Metastasis Assays

To count and measure macroscopic metastases, lungs were immersed in Bouin's solution (Sigma) for 24 hours and examined under a ×4 stereomicroscope. To examine metastases histologically, we resected lungs at the timepoints described, fixed tissue in 4% formaldehyde, and prepared 5-µm paraffin-embedded sections at 100-µm intervals throughout all lobes of all lungs. These were stained with hematoxylin and eosin, and metastases were counted by a trained pathologist. Metastasis area was determined using ImageJ software (National Institutes of Health). For experimental metastasis assays, 4T1 (1×10^6), E0771 (5×10^5), or *MMTV-PyVT* (5×10^5) cells were injected into the tail vein, and treatment commenced 12 hours later. Lung tissue was collected after fixation by intratracheal instillation of 4% paraformaldehyde (after 8 days' treatment for 4T1 and 5 days' treatment for E0771 and *MMTV-PyVT*). Three representative 5-µm sections (at least 100 µm apart) through each lobe of each lung were stained with hematoxylin and eosin and analyzed by a trained pathologist. Each tumor focus was graded as intra- or extravascular, and the number of cell nuclei visible at ×400 magnification in each focus was counted as a marker of tumor size.

Measurement of Tumor Hypoxia and Perfusion

Tumor hypoxia and perfusion were measured as previously described (12).

Radiotherapy

Tumor-bearing mice were anesthetized with ketamine and xylazine by intraperitoneal injection. Mice were secured in the supine position on a supportive platform using adhesive tape. A 6-mm thick 15-mm lead collimator was placed over the mammary fat pad tumor, and the mouse was placed into the irradiator (XRAD 320; Precision X-Ray, North Branford, CT). Radiation was directed at 3.52 Gy/min to a total of 20 Gy.

Statistical Analysis

Statistical analysis was performed using the unpaired *t* test. The χ^2 and Fisher exact tests were used as indicated to compare the relative distribution of metastatic events (by size or location). Repeated measures one-way analysis of variance was used for the analysis of primary tumor growth curves. Survival analysis was performed using the log-rank (Mantel–Cox) test. All statistical tests were two-sided. Differences were considered statistically significant at a *P* value less than .05.

See additional Materials and Methods in the Supplementary Materials (available online).

Results

Effect of AKB-9778, a VE-PTP Inhibitor, on Endothelial Tie-2 Signaling

In keeping with its activity as a VE-PTP inhibitor, AKB-9778 invoked rapid phosphorylation of tyrosine residues on the Tie-2 kinase in two EC lines (Figure 1A; Supplementary Figure 1A, available online), in turn activating known downstream pathways AKT and endothelial nitric oxide synthase (eNOS), the latter at the stimulatory Ser1177 residue (Figure 1B; Supplementary Figure 1B, available online). These effects were diminished when Tie-2 expression was knocked down in ECs using a *TIE2-shRNA* construct, establishing target specificity of AKB-9778 (Figure 1C; Supplementary Figure 1C, available online). In vivo, a single dose of AKB-9778 led to rapid phosphorylation of Tie-2 tyrosine residues in murine lung and mammary carcinoma tissue (Figure 1, D and E). Importantly, the activation of Tie-2 signaling in ECs in vitro was seen in the absence of Ang-1 and even in the presence of exogenous Ang-2 (Figure 1F).

Effect of AKB-9778 on EC Junctional Protein

The EC/EC adhesion molecule VE-cadherin has also been reported as a potential substrate for VE-PTP (either directly or through plakoglobin) (24). We found that although VE-PTP inhibition with AKB-9778 induced tyrosine phosphorylation of plakoglobin and VE-cadherin (Supplementary Figure 1, D and E, available online), the amount of VE-cadherin at the EC membrane was unchanged (Supplementary Figure 1G, available online). Moreover, there was no statistically significant indirect serine phosphorylation of VE-cadherin (a key determinant of its internalization) (Supplementary Figure 1F, available online).

Impact of VE-PTP Inhibition on Embryonic Angiogenesis

The *VE-PTP*$^{-/-}$ mouse is embryonically lethal because of defects in angiogenesis (25,26). Because the VE-PTP domains of *Danio rerio* and *Mus musculus* have high sequence homology, we evaluated the effects of AKB-9778 on embryonic vessels in *Flk1:GFP* zebrafish. We found specific effects on angiogenesis: intersegmental vessels appeared tortuous with reduced sprouting and at higher doses failed to reach the dorsal longitudinal anastomotic vessel at 48 hours postfertilization (Figure 2, A and B) ($P < .01$ by χ^2 test for Figure 2B). In addition, AKB-9778 reduced angiogenic sprouting into carcinoma xenografts growing in the avascular perivitelline space of zebrafish embryos ($P < .01$ by two-sided *t* test) (Figure 2, C and D; Supplementary Figure 2, A–C, available online).

Effect of VE-PTP Inhibition on Early-Stage Primary Tumor Vasculature and Growth

We next examined the effects of VE-PTP inhibition on pathological angiogenesis in breast cancer models in adult mice. First, we implanted 4T1 and E0771 murine mammary carcinoma cells in the mammary fat pad and initiated AKB-9778 treatment 24 hours later. AKB-9778 delayed the early phase of tumor growth in both models (Supplementary Figure 3, A–C, available online) but not the later phase of tumor growth. *VE-PTP* gene expression was not detectable in either tumor cell line by reverse-transcription polymerase chain reaction (not shown), and AKB-9778 had virtually no cytotoxic effects on these cells in vitro (median inhibitory concentration > 300 μM). Histologic examination of 4T1 tumors during this early phase of growth (tumor diameter < 1 mm) showed that AKB-9778 promoted vascular maturity, enhancing PVC coverage and proximity between PVCs and ECs (Supplementary Figure 3, D–F, available online).

Effect of VE-PTP Inhibition on the Growth of Spontaneous Micrometastases

To specifically study the effects of VE-PTP inhibition on metastasis, we used a model of spontaneous 4T1 mammary carcinoma metastasis and treated mice with AKB-9778 only after resecting primary tumors (ie, in an adjuvant therapy setting) (Figure 3A). AKB-9778 treated mice had a reduction in the number and size of macroscopic metastatic nodules in the lungs (control mean = 21.8 lung nodules per mouse, 95% confidence interval [CI] = 11.3 to 32.3; AKB-9778 mean = 8.6 lung nodules per mouse, 95% CI = 4.6 to 12.6; $P = 0.03$ by two-sided *t* test) and throughout the rest of the body, including liver, lymph nodes, and bones (Figure 3, B–E) (control mean = 26.7 total metastatic nodules per mouse, 95% CI = 15.5 to 37.9; AKB-9778 mean = 11.6 lung nodules per mouse, 95% CI = 6.1 to 17.1; $P = .03$ by two-sided *t* test). Detailed histologic assessment revealed that this effect was due to a delay in the growth but not in the number of metastases (Supplementary Figure 4, A–C, available online). These results show that VE-PTP inhibition delays the progression of micrometastases into macroscopic metastatic nodules.

Effect of VE-PTP Inhibition on Metastatic Tumor Cell Extravasation Into the Lungs

To determine if this effect of AKB-9778 on metastasis growth was specifically due to improved vessel stabilization by Tie-2 activation, we used an experimental metastasis model. 4T1 cells, known to have an extended intravascular growth phase after homing to the lungs, were intravenously injected, and AKB-9778 treatment commenced 24 hours later. After 8 days, the lungs of

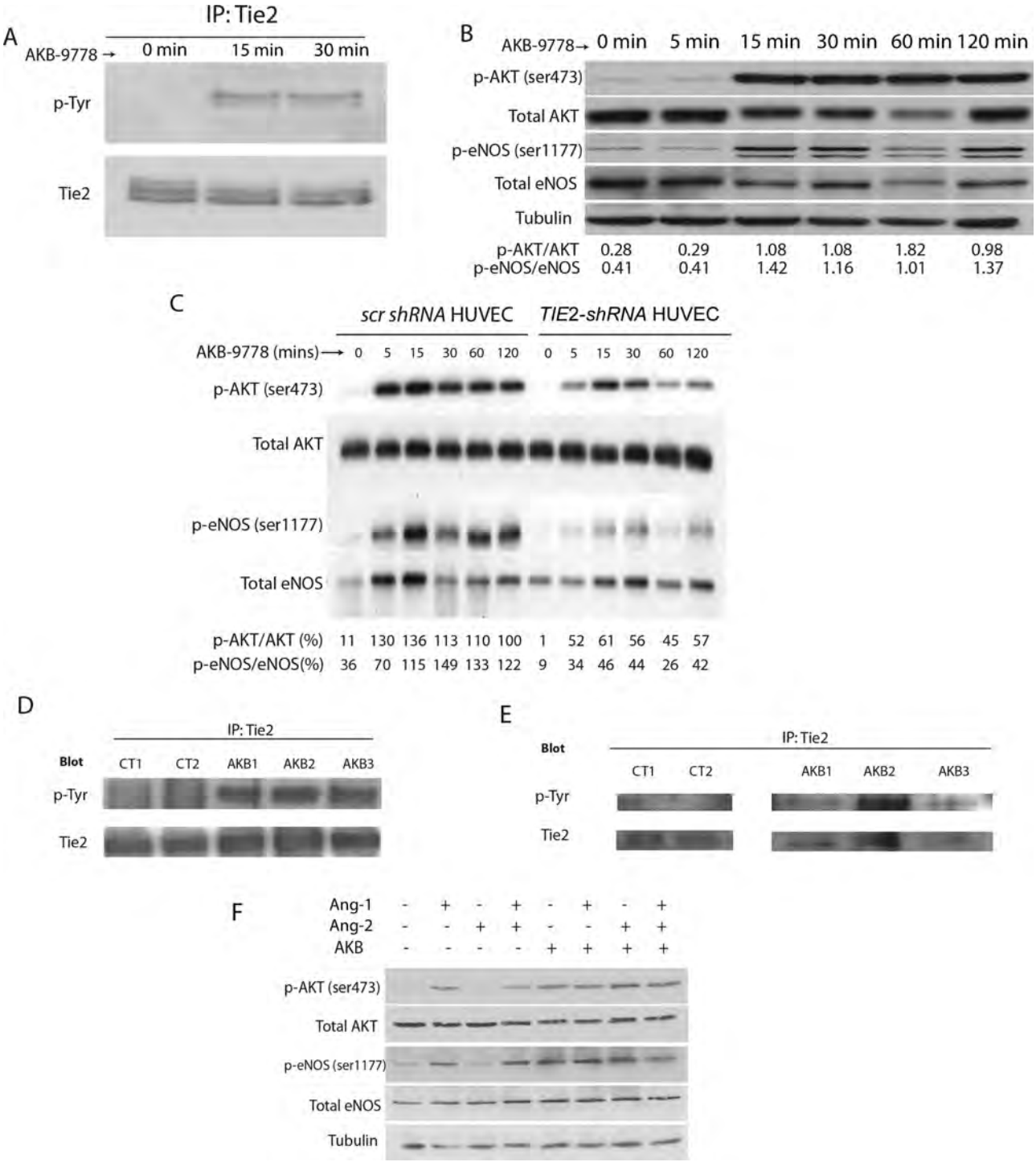

Figure 1. Effect of AKB-9778, a vascular endothelial protein tyrosine phosphatase (VE-PTP) inhibitor, on Tie-2 signaling in endothelial cells. **A**) Tie-2 tyrosine phosphorylation in human umbilical vein endothelial cell (HUVEC) lysates after AKB-9778 treatment. **B**) Levels of phosphorylated AKT (Ser473), total AKT, phosphorylated endothelial nitric oxide synthase (eNOS) (Ser1177), and total eNOS in HUVEC lysates after treatment with AKB-9778 (numbers below blot indicate densitometric ratios as labeled). **C**) Phosphorylated AKT (Ser473 residue), total AKT, phosphorylated eNOS (Ser1177 residue), and total eNOS levels in HUVEC lysates or *TIE2-shRNA* HUVEC lysates after exposure in vitro to AKB-9778 (numbers below blot indicate densitometric ratios as labeled). **D**)Tie-2 tyrosine phosphorylation in murine whole lung lysates 1 hour after intravenous injection of AKB-9778 or control vehicle. **E**) Tie-2 tyrosine phosphorylation in murine orthotopic 4T1 mammary carcinoma lysates 1 hour after intravenous injection of AKB-9778 or control vehicle. **F**) Levels of phosphorylated AKT (Ser473), total AKT, phosphorylated eNOS (Ser1177), and total eNOS in HUVEC lysates after 30 minutes of treatment with angiopoietin 1 (Ang-1), angiopoietin 2 (Ang-2), and/or AKB-9778.

AKB-9778-treated mice showed statistically significantly smaller micrometastases (Supplementary Figure 5A, available online) ($P < .01$ by two-sided t test). Histologically, AKB-9778–treated mice showed clumps of metastatic cells lodged within alveolar vessels that failed to breach the vascular basement membrane and enter the lung parenchyma (Figure 4, A–C) (statistically

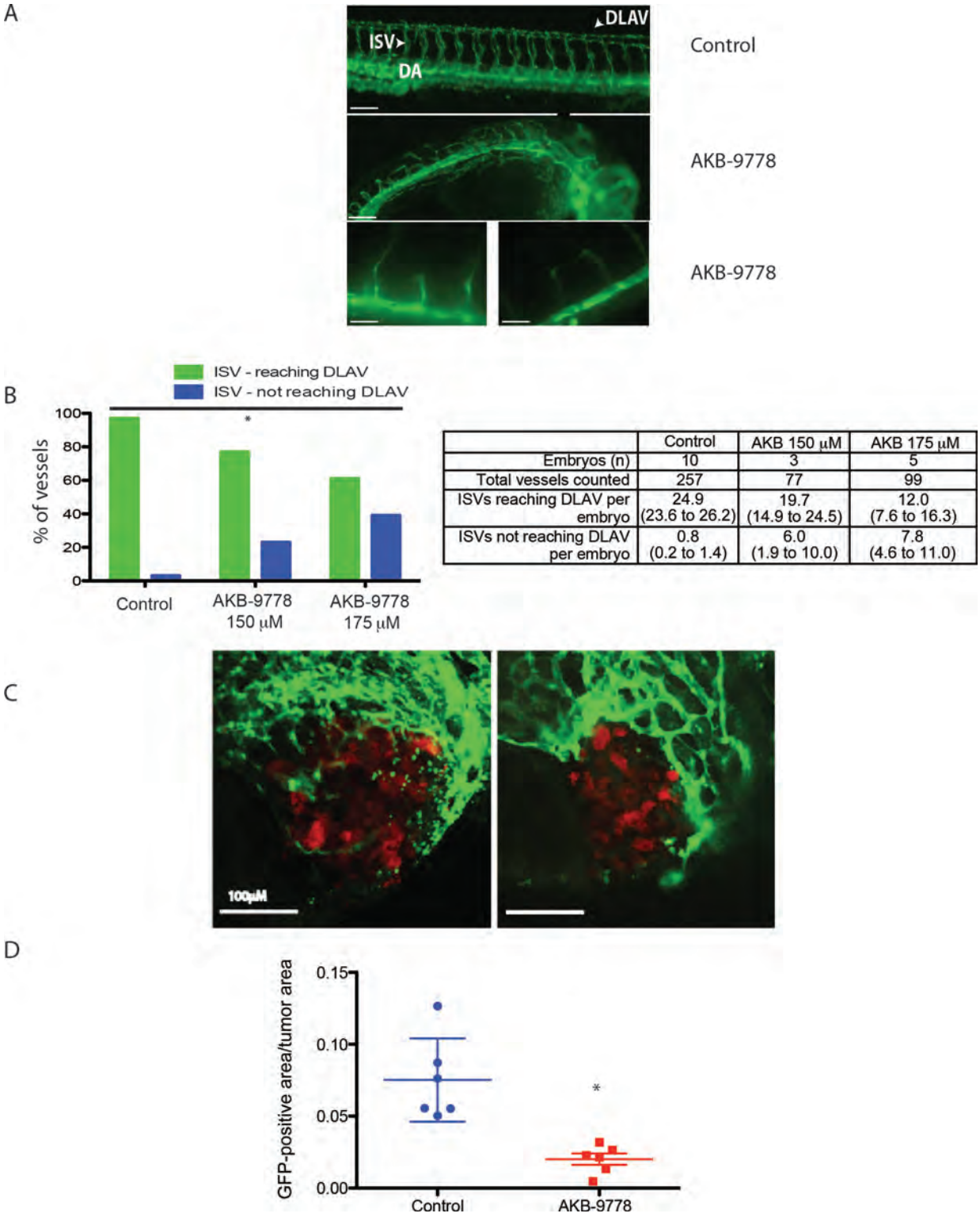

	Control	AKB 150 μM	AKB 175 μM
Embryos (n)	10	3	5
Total vessels counted	257	77	99
ISVs reaching DLAV per embryo	24.9 (23.6 to 26.2)	19.7 (14.9 to 24.5)	12.0 (7.6 to 16.3)
ISVs not reaching DLAV per embryo	0.8 (0.2 to 1.4)	6.0 (1.9 to 10.0)	7.8 (4.6 to 11.0)

Figure 2. Effect of vascular endothelial protein tyrosine phosphatase (VE-PTP) inhibition on embryonic and tumor angiogenesis in zebrafish. **A**) Representative epifluorescence micrographs of *Flk-1:GFP* zebrafish embryos treated with control vehicle (DMSO) (**top panel**) or AKB-9778 (**middle panel**) at 48 hours postfertilization. **Lower panels** (left and right) show high-powered images of AKB-9778–treated embryos at 48 hours postfertilization. DLAV = dorsal longitudinal anastomotic vessel; DA = dosal aorta; ISV = intersegmental vessel. Scale bars: top panel = 100 μm; middle panel = 75 μm; bottom panels = 50 μm. **B**) Percentage of vessels that sprouted from the dorsal aorta to reach the dorsal longitudinal anastomotic vessel in zebrafish embryos treated with control vehicle (DMSO) or AKB-9778 (*$P < .01$ by χ^2 test; n = 5–6 embryos per group). Table shows total vessels counted with data as means and 95% confidence intervals (CIs). **C**) 4T1-dsRed mammary carcinomas growing in *Flk-1:GFP* zebrafish embryos treated with control vehicle (**left panel**) or AKB-9778 (**right panel**). **D**) Vessel density (determined as green fluorescent protein [GFP]-positive area/tumor area) from experiment in (**C**) (*$P < .01$ by two-sided t test; n = 6 embryos per group). Value for each embryo is determined as the mean of five individual micrographs taken throughout each tumor. **Bars** show mean ± standard deviation (control mean = 0.08, 95% CI = 0.04 to .11; AKB-9778 mean = 0.02, 95% CI = 0.01 to 0.03).

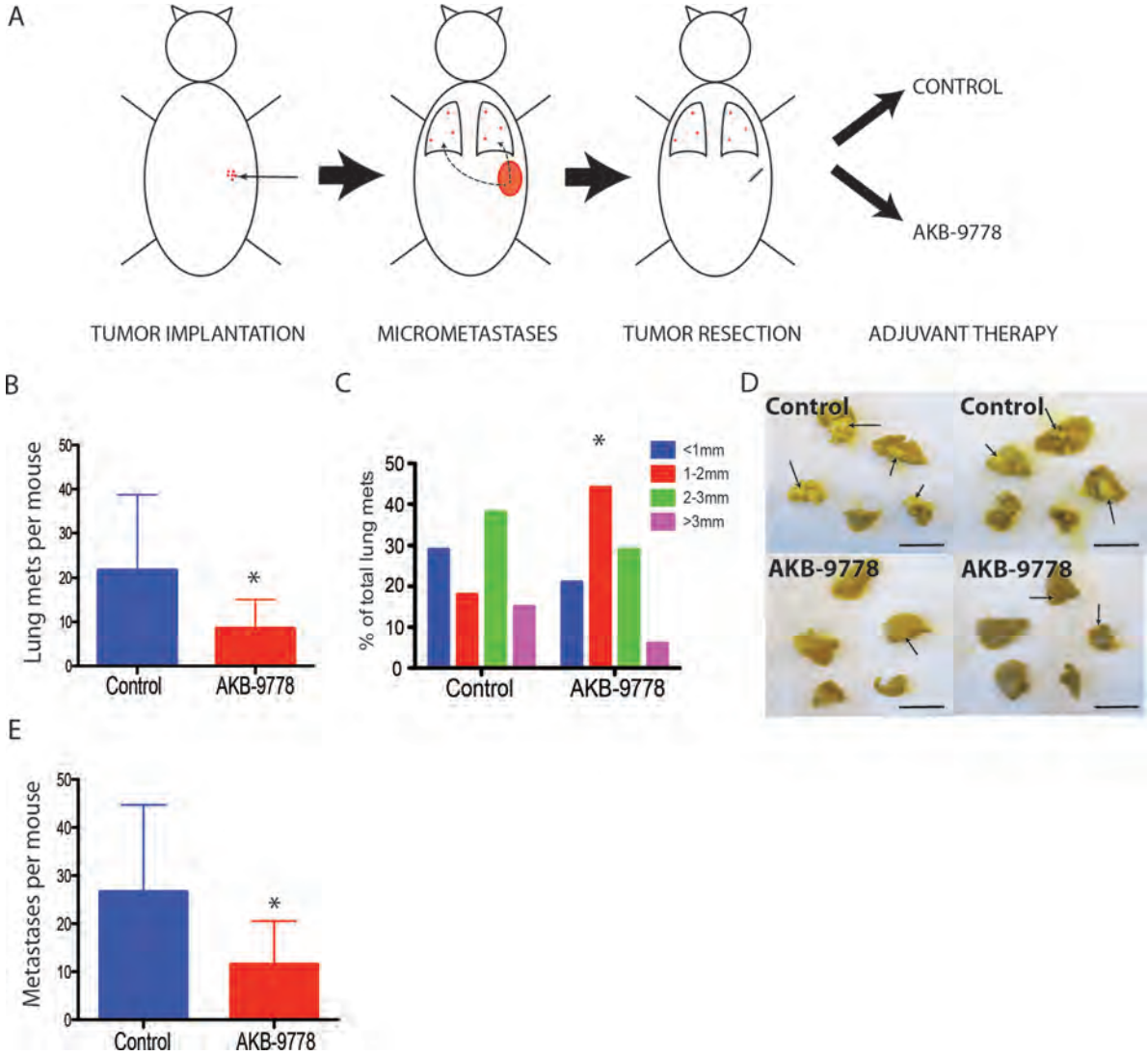

Figure 3. Impact of adjuvant therapy with AKB-9778 on the growth of spontaneous micrometastases. **A**) Schema demonstrating model for adjuvant AKB-9778 therapy. Orthotopically grown 4T1 tumors were resected at 5 mm in diameter. **B**) Number of macroscopic lung metastases in control vs AKB-9778–treated mice (*P = .03 by two-sided t test; n = 10 per group) after 3 weeks of treatment. **C**) Distribution of the size of macrometastatic lung nodules (*P < 0.01 by two-sided χ^2 test). **D**) Representative images of lungs visualized after resection in control (**upper panels**) and AKB-9778 treated (**lower panels**) mice (**scale bars** = 10 mm). **E**) Total number of macroscopically detected metastases (including lung, liver, bone, lymph node, and soft tissue) (*P = .03 by two-sided t test; n = 10 per group). For all panels, **error bars** represent standard deviation.

significantly more intravascular metastases seen in the AKB-9778 group, P < .01 by two-sided Fisher exact test). Similar results were seen after injecting E0771 cells and tumor cells isolated from *MMTV-PyVT* spontaneously arising tumors intravenously into syngeneic mice and examining the lungs after 5 days of treatment (Figure 4D; Supplementary Figure 5, B–D, available online).

Given the finding that AKB-9778 delays extravasation of metastatic tumor cells into the lungs and slows progression of micrometastases, we asked if adjuvant AKB-9778 therapy in the 4T1 spontaneous metastasis model could improve outcomes beyond a standard cytotoxic therapy. Indeed, there was a strong trend toward improved overall survival from the addition of AKB-9778 to adjuvant doxorubicin chemotherapy from 27.0 to 36.5 days in this model (hazard ratio for overall survival = 0.33, 95% CI = 0.11 to 1.03; P = .05 by Mantel–Cox test) (Figure 4E).

Effects of VE-PTP Inhibition on the Structure and Function of Established Primary Tumor Vessels

Next, we examined the effects of VE-PTP inhibition on the vasculature of established primary tumors that would have already passed through the "angiogenic switch" (commencing treatment at tumor diameter 3 mm). In both 4T1 and E0771 breast tumor models, AKB-9778 therapy led to more structurally mature tumor vessels, evidenced by increased PVC coverage (Figure 5, A, B, D, E) and a greater proximity between PVCs and ECs (Figure 5C) (control mean distance between PVC and EC = 0.90 μM, 95% CI = 0.87 to 0.93 μM; AKB-9778 mean distance between PVC and EC = 0.79 μM, 95% CI = 0.74 to 0.84 μM). Also consistent with the known effects of Tie-2 activation (10,11,27), AKB-9778–treated tumors showed an increase in vessel diameter and vessel density in both tumor models (Figure 5, F–I) (in 4T1, control vessel diameter mean = 10.4 μM, 95% CI = 10.0 to 10.9 μM, and

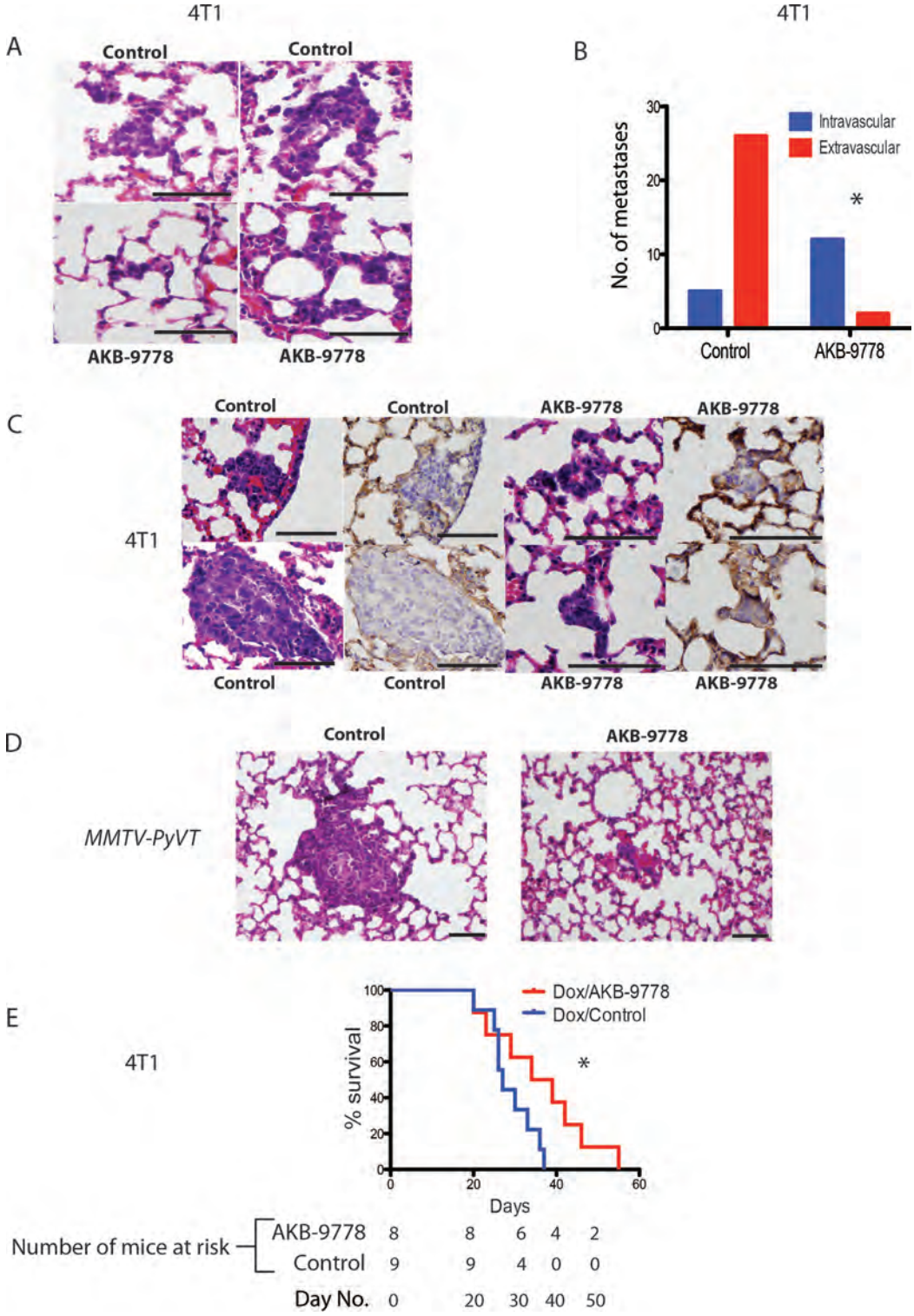

Figure 4. Effect of vascular endothelial protein tyrosine phosphatase (VE-PTP) inhibition on extravasation of disseminated tumor cells into distant organ parenchyma. **A–C**) 4T1 mammary carcinoma cells were injected intravenously, and therapy with control or AKB-9778 commenced 12 hours later. Lungs were examined for micrometastases after 8 days. **A**) Representative hematoxylin and eosin–stained sections of micrometastases. Control lungs (**upper panels**) show micrometastatic cells that have breached vascular boundaries and entered the alveolar airspace. AKB-9778–treated lungs (**lower panels**) show cells tracking within vessels yet to extravasate (**scale bars** = 100 μm). **B**) Number of intra- vs extravascular micrometastases (*P < .01 by two-sided Fisher exact test; n = 6 mice per group; data show total number of metastases combined for all mice in each group). **C**) Representative images of micrometastases. Images show hematoxylin and eosin–stained sections of micrometastases and serial sections (separated by 5 microns) showing the same metastasis stained for collagen IV (**brown**). Control mice show extravasation of tumor cells through the vascular basement membrane, but AKB-9778–treated mice show tumor cells retained within vessels (**scale bars** = 100 μm). **D**) Representative images of experimental *MMTV-PyVT* tumor cell micrometastases treated with control (**left panel**) or AKB-9778 (**right panel**) (**scale bars** = 100 μm). **E**) Mouse survival after adjuvant therapy with doxorubicin ± AKB-9778. (*P = .05 using log-rank [Mantel–Cox] test; n = 8–9 mice per group) using a model of 4T1 spontaneous metastasis.

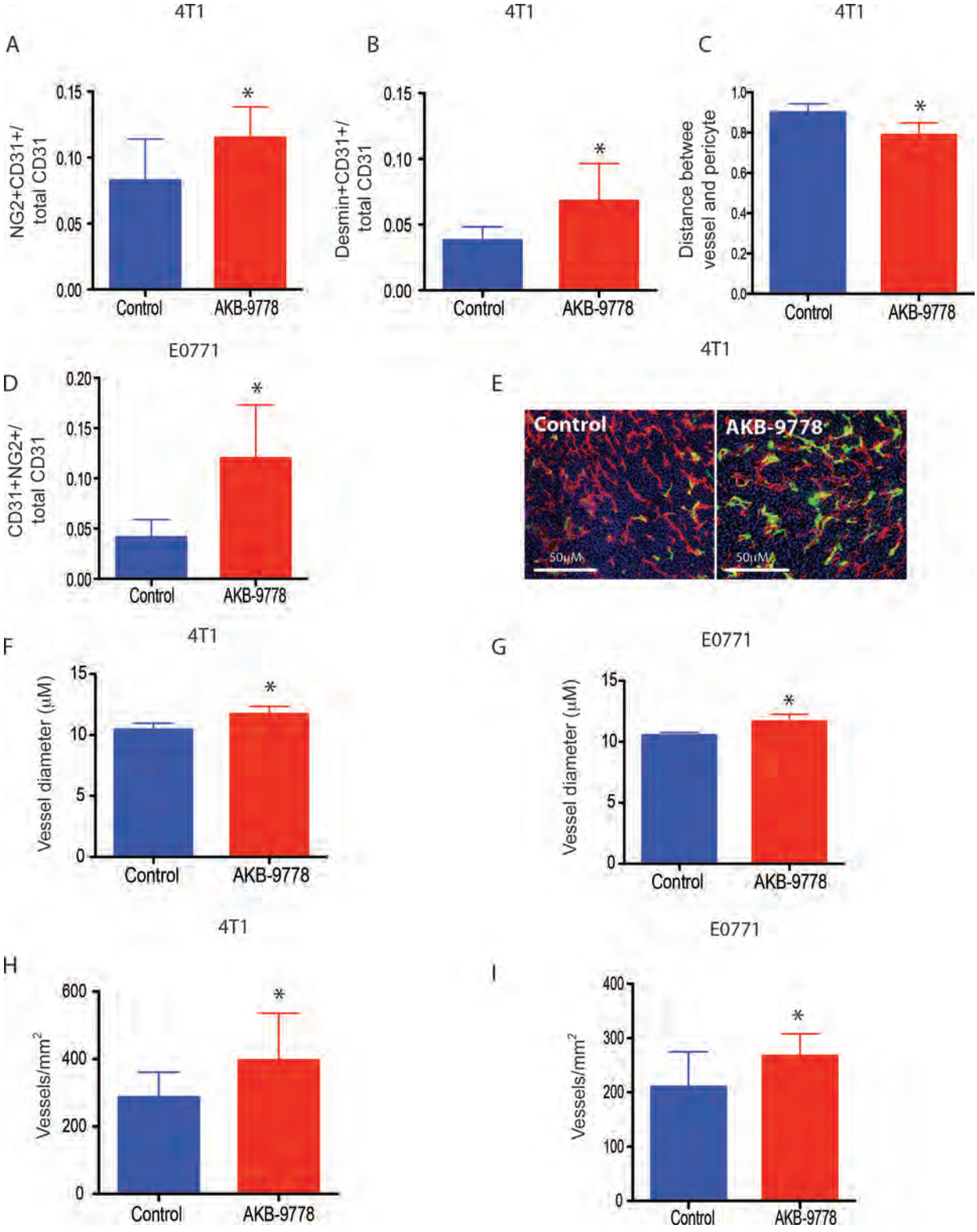

Figure 5. Structural changes within established primary tumor vessels invoked by vascular endothelial protein tyrosine phosphatase (VE-PTP) inhibition. **A**) Colocalization of CD31-positive area (endothelial cells) and NG2-positive area (perivascular cells) (*P = .05 by two-sided t test; n = 6 per group) in 4T1 tumors. **B**) Colocalization of CD31-positive area (endothelial cells) and desmin-positive area (perivascular cells) (*P = .01 by two-sided t test; n = 6 per group) in 4T1 tumors. **C**) Mean distance between desmin-positive pericytes and CD31=positive endothelial cells in microns (*P < .01 by two-sided t test; n = 6 per group) in 4T1 tumors. **D**) Colocalization of CD31+ area (endothelial cells) and NG2+ area (perivascular cells) (*P = .05 by two-sided t test; n = 6 per group) in E0771 tumors (*P < .01 by two-sided t test; n = 6 per group). **E**) Enhanced vascular pericyte coverage in AKB-9778–treated tumors (**right panel**) compared with control-treated tumors (**left panel**) (**red**: CD31; **green**: NG2; **blue**: DAPI). **F–G**) Vessel diameter in control vs AKB-9778–treated 4T1 (**F**) and E0771 (**G**) tumors (**F**: *P < .01 by two-sided t test, n = 6 per group; **G**: *P < .01 by two-sided t test, n = 6 per group). **H–I**) Vessel density in control vs AKB-9778–treated 4T1 (**H**) and E0771 (**I**) tumors (**H**: *P = .05 by two-sided t test, n = 6 per group; **I**: *P = .05 by two-sided t test, n = 6 per group). **Error bars** represent standard deviation for all panels.

AKB-9778 vessel diameter mean = 11.7 μM, 95% CI = 11.2 to 12.2 μM, P = .003 by two-sided t-test; in E0771, control vessel diameter mean = 10.5 μM, 95% CI = 10.4 to 10.7 μM, and AKB-9778 vessel diameter mean = 11.7 μM, 95% CI = 11.2 to 12.1 μM, P < .01 by two-sided t test). Consistent with our in vitro data, total VE-cadherin levels in tumor ECs were unchanged after 9 days of AKB-9778 therapy (Supplementary Figure 6A, available online).

We next assessed the function of vessels in established primary tumors after treatment with AKB-9778. First, AKB-9778 reduced tumor microvascular permeability in keeping with Tie-2 activation (Figure 6, A and B) (mean increase in permeability from baseline to day 4 of treatment was 182% for control [95% CI = 85% to 280%] and 13% for AKB-9778 [95% CI = –4% to 30%); P = .03 by two-sided t test). In addition, overall tumor perfusion was increased in both 4T1 and E0771 tumors after AKB-978 therapy (Figure 6, C–F; Supplementary Figure 6B, available online) as measured by ex vivo measurement of perfusion by intravenously injected lectin. Intravital optical frequency domain imaging (28) confirmed enhanced tumor perfusion in 4T1 carcinomas after treatment with AKB-9778 (Figure 6I). This increase in blood perfusion led to a reduction in tumor hypoxia, assessed by redox marker staining (Figure 6, G and H). Of note, VE-PTP inhibition did not accelerate the growth of any of four different orthotopic mammary carcinoma models tested, including spontaneously arising *MMTV-PyVT* tumors (Supplementary Figure 7, A–D, available online).

Given the observed reduction in hypoxia, we then studied the effect of AKB-9778 pretreatment on the efficacy of tumor radiotherapy. Pretreating orthotopic mammary 4T1 tumors with AKB-9778 led to a modestly enhanced growth delay from subsequent radiotherapy (time to tumor doubling in volume after radiotherapy prolonged by approximately 2.5 days; P <.01 by analysis of variance when comparing radiotherapy alone and AKB plus radiotherapy groups). Given that AKB-9778 monotherapy had no effect on tumor growth in this setting, these data indicate tumor radiosensitization by AKB-9778 pretreatment (Figure 6J).

Systemic Effects of AKB-9778 Therapy

We next examined the effects of AKB-9778 therapy on the structure and function of nontumor vessels. In healthy non-tumor-bearing mice, AKB-9778 reduced cutaneous vessel permeability as assessed by the Miles assay and increased cutaneous vessel diameter after 48 hours of treatment, consistent with Tie-2 activation (Supplementary Figure 8, A and B, available online). Despite the observed increase in vessel diameter, there was no change in systemic blood pressure after AKB-9778 treatment of tumor-bearing mice (Supplementary Figure 8C, available online).

Role of eNOS in Mediating VE-PTP–induced Tumor Vascular Alterations

We have previously found that recreating nitric oxide gradients around the tumor vascular endothelium mediates angiogenesis and vessel maturation, improving tissue perfusion and oxygenation (29,30). Given our finding that AKB-9778 increases phosphorylation of EC eNOS at the Ser1177 residue (Figure 1B), we next examined whether the improved perfusion seen after VE-PTP inhibition in established primary tumors is due to heightened eNOS activity. Importantly, neither AKB-9778 nor recombinant Ang-1 enhanced phosphorylation at the inhibitory Thr495 eNOS residue in ECs (Supplementary Figure 9, available online). Consistent with this, AKB-9778 induced a marked increase in EC nitric oxide production in vitro that was abolished by an NOS inhibitor (Figure 7, A and B). When administered to eNOS-deficient (*Nos3*$^{-/-}$) mice bearing established orthotopic E0771 breast carcinomas, AKB-9778 therapy had no effect on tumor growth, which is consistent with previous experiments in this late treatment setting in wild-type mice (Figure 7C). Unlike wild-type mice tumors, however, we did not observe an increase in vessel density or diameter by AKB-9778 treatment in *Nos3*$^{-/-}$ mice, suggesting that the effects of VE-PTP inhibitor are at least in part mediated by eNOS (Figure 7, D and E) (29).

Discussion

In this study, we show that pharmacological inhibition of the VE-PTP domain stabilizes tumor vessels through activation of the EC Tie-2 kinase. Using AKB-9778, a novel, first-in-class VE-PTP inhibitor, we showed direct benefits of VE-PTP inhibition in several stages of tumor progression including metastasis.

As a VE-PTP inhibitor, AKB-9778's capacity to activate the Tie-2 kinase is in keeping with previous work demonstrating that inhibition of VE-PTP expression by antibodies, small interfering RNA, or gene disruption triggers Tie-2 tyrosine phosphorylation in ECs (20). Furthermore, the angiogenic defects observed in *VE-PTP*$^{-/-}$ mouse embryos (attributed to Tie-2 hyperactivation) are recapitulated by AKB-9778 in our zebrafish embryonic angiogenesis assays (25,26).

Importantly, the extracellular domain of VE-PTP associates with VE-cadherin. Nottebaum et al. have shown that VE-PTP might be important in maintaining EC junctional integrity through a mechanism requiring plakoglobin and VE-cadherin (24). Although we observed increased tyrosine phosphorylation of both plakoglobin and VE-cadherin in ECs after AKB-9778 exposure, we found no change in VE-cadherin subcellular localization in vitro or in total VE-cadherin levels in tumor ECs in vivo after prolonged AKB-9778 treatment. Moreover, the observed reductions in vascular permeability are consistent with Tie-2 activation rather than impaired EC junctional integrity. Collectively, these data show that the effects of pharmacological VE-PTP domain inhibition are mediated primarily through increased Tie-2 kinase activity.

The ligand-independent activity of AKB-9778 is an attractive property and is relevant when comparing anti-Ang-2 therapies to VE-PTP inhibition. First, inter- and intratumor levels of Ang-2 are highly variable (31), and anti-Ang-2 strategies can only be effective in tumors and regions that express sufficient levels of Ang-2. In contrast, we show that VE-PTP inhibition activates Tie-2 regardless of ligand context. Second, because tumors typically express higher levels of Ang-2 than Ang-1 (15), Ang-2 blockade may not necessarily lead to Tie-2 activation in tumor ECs. In contrast, VE-PTP inhibition consistently activates Tie-2 and its downstream effector pathways, even in the presence of Ang-2.

Early in primary tumor development, cancer cells co-opt host vessels that then upregulate production of Ang-2 (6) and VE-PTP (26), presumably leading to Tie-2 deactivation, vessel destabilization, and sprouting angiogenesis (6). Our observation that

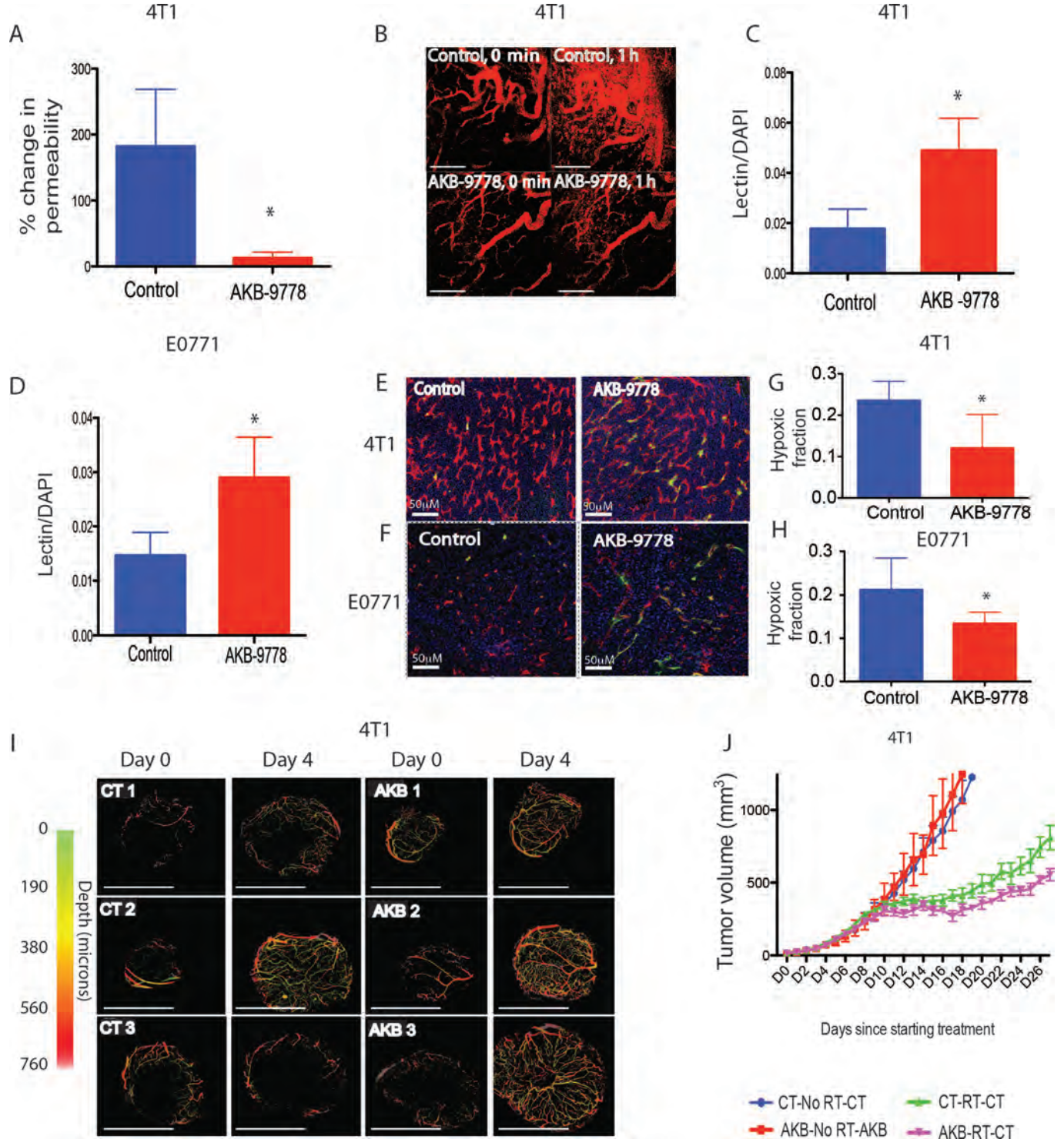

Figure 6. Effect of vascular endothelial protein tyrosine phosphatase (VE-PTP) inhibition on tumor vessel function, hypoxia, and radiosensitivity. **A**) Percentage change in permeability from baseline to after 72 hours of treatment in control vs AKB-9778–treated 4T1 tumors (*P = .03 by two-sided t test; n = 3 per group). **B**) Intravital micrographs taken 0 minutes and 1 hour after intravenous injection of fluorescent bovine serum albumin after treatment with control (**top panels**) or AKB-9778 (**lower panels**) (**scale bars** = 200 μm). **C** and **D**) Lectin positive area in control vs AKB-9778–treated 4T1 (**C**) and E0771 (**D**) tumors (**C**: *P = .03 by two-sided t test, n = 6 per group; **D**: *P = .05 by two-sided t test, n = 5 per group). **E** and **F**) Enhanced vessel perfusion by lectin in AKB-9778–treated tumors (**lower panel**) compared with control (**upper panel**) (**E**: 4T1l; **F**: E0771). **G** and **H**) Relative hypoxic fraction assessed by pimonidazole staining in control vs AKB-9778–treated 4T1 (**G**) and E0771 (**H**) tumors (**G**: *P = .05 by two-sided t test, n = 10–13 per group; **H**: *P = .04 by two-sided t test, n = 9–10 per group). For (**A**) and (**B**), data were obtained after 72 hours of treatment, and for (**C**–**H**), treatment was commenced at tumor diameter of 3 mm and continued for 10 days. **I**) Intravital optical frequency domain imaging of 4T1 mammary carcinomas at baseline (day 0, diameter 2–3 mm) and after 4 days of treatment with AKB-9778 or control vehicle. Images show perfused vessels only. **Scale bars** represent 4 mm. **J**) 4T1 tumor growth curves from combined AKB-9778 and radiotherapy. Treatment was begun at diameter 3 mm, and radiotherapy given 1 week later (*P < .01 comparing **green and pink lines** by analysis of variance; n = 7 per group). For all panels, **error bars** represent standard deviation.

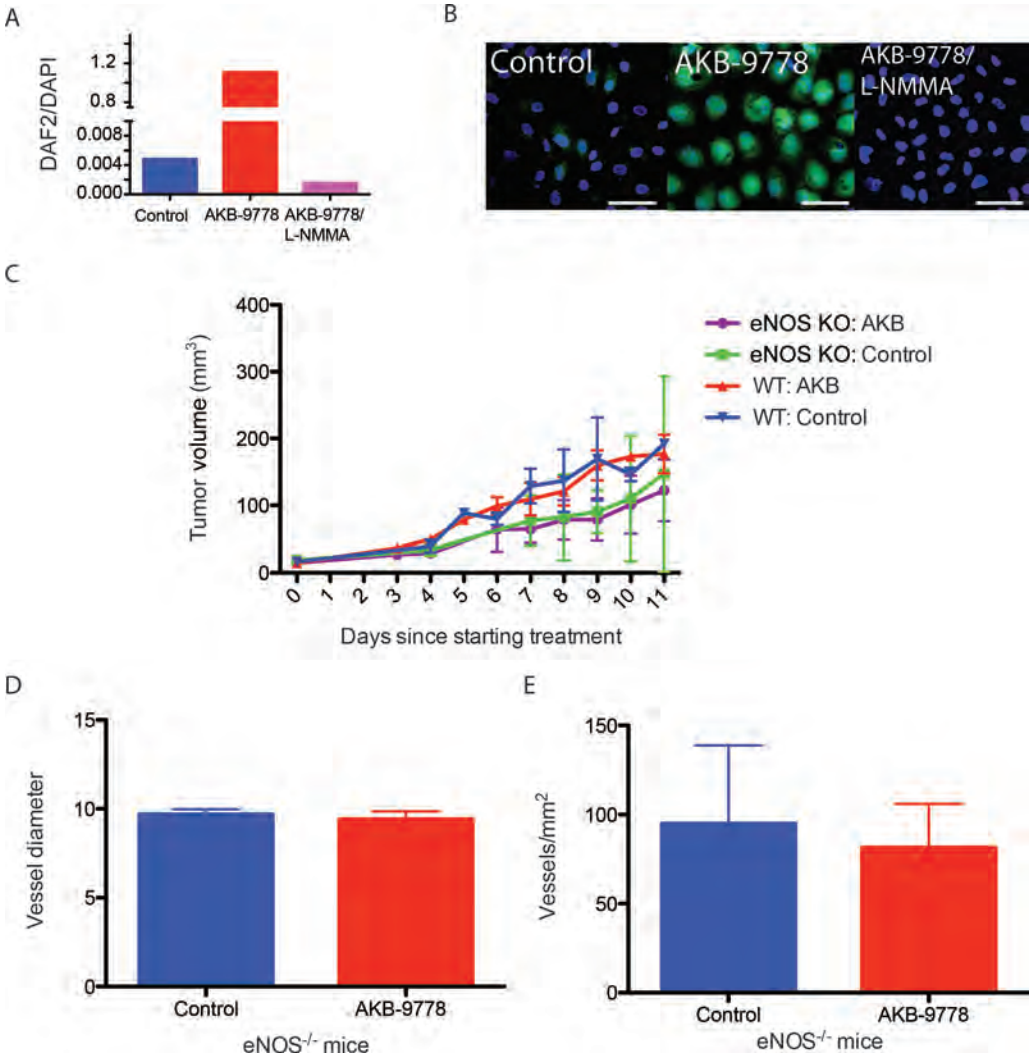

Figure 7. Role of endothelial nitric oxide synthase in vascular endothelial protein tyrosine phosphatase (VE-PTP)–induced tumor vascular alterations. **A**) Human umbilical vein endothelial cell (HUVEC) nitric oxide production in vitro after treatment with control, AKB-9778, or N^G-Monomethyl-L-arginine (L-NMMA). Nitric oxide production was determined by quantification of the fluorescent signal from DAF-2T. **B**) Representative images of DAF-2T fluorescence (**green**) in HUVECs after treatment with control (**left panel**), AKB-9778 (**center panel**), or AKB-9778 and L-NMMA (**right panel**) (**scale bars** = 20 μM). **C**) E0771 mammary carcinoma was implanted orthotopically into either wild-type (WT) C57Bl/6 mice or *NOS3*$^{-/-}$ mice (KO). At tumor diameter of 3 mm, mice were treated with either AKB-9778 or control vehicle (n = 5 per group). Data show tumor growth curves. eNOS = endothelial nitric oxide synthase. **D**) Vessel diameter in E0771 orthotopic mammary carcinomas treated with AKB-9778 or control vehicle in *NOS3*$^{-/-}$ mice (P = .40 by two-sided t test; n = 5 per group). **E**) Vessel density in E0771 orthotopic mammary carcinomas treated with AKB-9778 or control vehicle in *NOS3*$^{-/-}$ mice (P = .77 by two-sided t test; n = 5 per group). For all panels, **error bars** represent standard deviation.

inhibition of the VE-PTP during this time stabilizes host vessels and delays the early phase of primary tumor growth is consistent with the results seen when growing tumors in Ang-2–deficient mice (32).

The early phase of tumor growth is most clinically relevant to the progression of micrometastases to macroscopic tumors. Metastatic cells that home to distant organs subsequently adhere to ECs that in turn upregulate Ang-2 (6). The resultant vessel destabilization facilitates extravasation subsequent and micrometastatic colonization of cells into distant organs (33,34). Here, we show that Tie-2 activation through VE-PTP inhibition constrains metastatic tumor cells to the distant organ's intravascular compartment, hence slowing metastatic progression. Previous studies have shown a reduction in spontaneous metastasis using Ang-2 blockade (14,15). In those models, however, anti-Ang-2 monotherapy or anti-Ang-2/VEGF double therapy statistically significantly delayed primary tumor growth, which could in itself delay metastasis. By using a spontaneous metastasis model where therapy was only begun after resection of the primary tumor, we show that VE-PTP inhibition delays progression of existing micrometastases to macrometastases and prolongs mouse survival. Furthermore, our experimental metastasis models confirm inhibition of the extravasation step of the metastatic cascade after VE-PTP inhibition. In prior preclinical studies, it has been suggested that surgical removal of a primary tumor may remove an angio-inhibitory stimulus upon micrometastases, promoting their progression through neovascularization (35). Therefore, further studies examining the role of perioperative AKB-9778 therapy are warranted.

We also observed structural and functional normalization of vessels after AKB-9778 therapy of established tumor vessels. Our

results are in part supported by a previous study showing that *VE-PTP* gene silencing in embryonic stem cell–derived tumors increases vessel diameter (27). As we have previously shown (12), anatomically small differences in vascular structure (such as increased PVC-EC proximity and increased vessel diameter) can have profound effects of normalizing vascular function. The accompanying increase in tumor perfusion and reduction in hypoxia are clinically relevant: reduced tumor perfusion and tumor hypoxia are known determinants of aggressive tumor behavior, insensitivity to chemo- and radiotherapy, and a poor prognosis (9,36,37). By activating Tie-2 signaling, VE-PTP inhibition reduces hypoxia and improves radiotherapy efficacy. These effects differ from those previously observed from anti-Ang-2 therapies of solid tumors, which characteristically result in narrowed vessels with an increase in tumor hypoxia (15,17). This may relate to the previously discussed differences between anti-Ang-2 therapy and VE-PTP inhibition on the state of Tie-2 activity. Although the goal of sustained improvement in perfusion and oxygenation has previously been realized through the use of genetic mouse models (3,38), gene targeting (4), and cytokine therapy (39), we present here a novel approach to achieve similar effects using a low molecular weight pharmacological agent.

Our observation that Tie-2 activation by VE-PTP inhibition increases eNOS phosphorylation at its stimulatory Ser1177 residue with no accompanying increase in Thr495 phosphorylation stands in contrast to a previous report (40) but is consistent with eNOS biology, where counter-regulatory residues are typically phosphorylated/dephosphorylated in a manner that yields a unidirectional effect on enzyme activity. The resultant increase in EC nitric oxide production is also in keeping with these findings. We have previously demonstrated that concentrating intratumoral nitric oxide around the endothelial compartment normalizes tumor vessel structure and function, improving perfusion and reducing hypoxia (29,30), and here we show that eNOS mediates vessel density and diameter increases by AKB-9778. Further studies are required to fully understand the involvement of eNOS

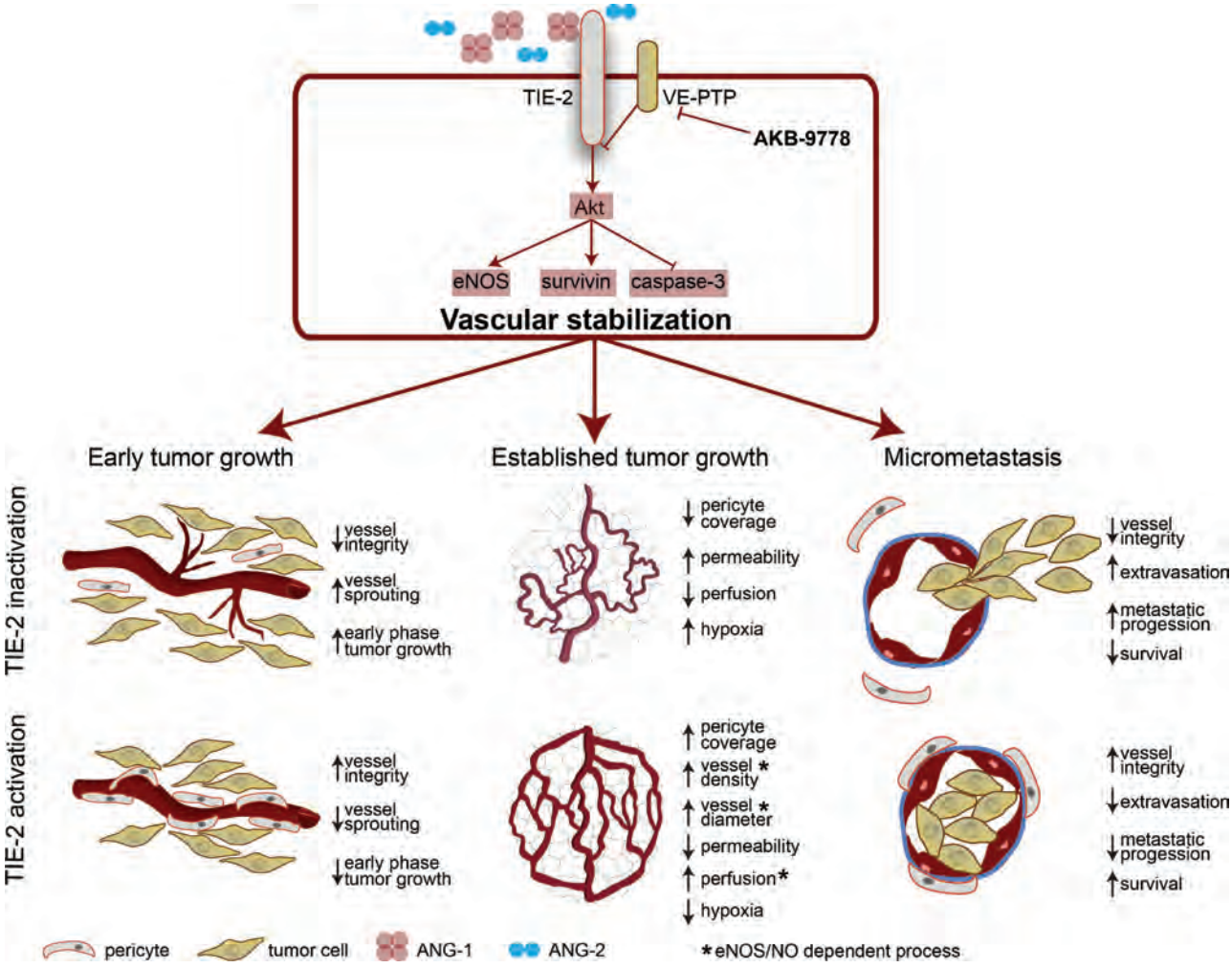

Figure 8. The effects of vascular endothelial protein tyrosine phosphatase (VE-PTP) inhibition in mouse models of breast cancer. Inhibition of the VE-PTP domain in endothelial cells activates Tie-2 signaling, in turn promoting a more stable vessel phenotype. In early tumor growth, this prevents early destabilization and hence slows the initial phase of tumor progression. In established tumors, vessels show structural and functional changes of normalization, resulting in improved tumor perfusion (which occurs because of an increased production of nitric oxide [NO] by endothelial nitric oxide synthase [eNOS]). In the setting of micrometastasis, stabilization of distant organ vessels prevents extravasation of tumor cells, delaying micrometastatic progression and prolonging survival.

in AKB-9778's effects on blood vessels, tumor progression, and dissemination.

There are, however, a number of limitations in our study. First, further work is needed to validate the importance of VE-PTP in human solid tumors. Second, it will be important to see whether results similar to what we saw in mammary tumors are reproduced in models of other tumor types. Third, further studies in spontaneously arising tumors, which may more faithfully replicate the tumor vessel phenotype, are warranted because the majority of our current data comes from models using implantable tumors from murine cell lines. Finally, we acknowledge that the understanding of VE-PTP biology and targets remains an emerging field, and the vascular effects should be evaluated as new potential targets for the phosphatase are discovered.

In summary, we propose sustained Tie-2 activation by VE-PTP inhibition as a novel approach to tumor vascular normalization (Figure 8). Unlike the majority of small molecule–targeted therapies that inhibit tyrosine kinases, AKB-9778 works to increase Tie-2 kinase activity and hence stabilizes vessels and normalizes their function. VE-PTP inhibition has not been reported in any disease model before, but first-in-human dose-finding studies with AKB-9778 are now complete (41). Our data provide novel biological insights into the role of VE-PTP in tumor initiation, progression, metastasis, and treatment.

References

1. Endrich B, Reinhold HS, Gross JF, Intaglietta M. Tissue perfusion inhomogeneity during early tumor growth in rats. *J Natl Cancer Inst*. 1979;62(2):387–395.
2. Jain RK. Normalizing tumor vasculature with anti-angiogenic therapy: a new paradigm for combination therapy. *Nat Med*. 2001;7(9):987–989.
3. Mazzone M, Dettori D, Leite de Oliveira R, et al. Heterozygous deficiency of PHD2 restores tumor oxygenation and inhibits metastasis via endothelial normalization. *Cell*. 2009;136(5):839–851.
4. Leite de Oliveira R, Deschoemaeker S, Henze AT, et al. Gene-targeting of phd2 improves tumor response to chemotherapy and prevents side-toxicity. *Cancer Cell*. 2012;22(2):263–277.
5. Weis SM, Cheresh DA. Pathophysiological consequences of VEGF-induced vascular permeability. *Nature*. 2005;437(7058):497–504.
6. Holash J, Maisonpierre PC, Compton D, et al. Vessel cooption, regression, and growth in tumors mediated by angiopoietins and VEGF. *Science*. 1999;284(5422):1994–1998.
7. Dvorak HF. Tumors: wounds that do not heal. Similarities between tumor stroma generation and wound healing. *N Engl J Med*. 1986;315(26):1650–1659.
8. Goel S, Duda DG, Xu L, et al. Normalization of the vasculature for treatment of cancer and other diseases. *Physiol Rev*. 2011;91(3):1071–1121.
9. Jain RK. Normalization of tumor vasculature: an emerging concept in antiangiogenic therapy. *Science*. 2005;307(5706):58–62.
10. Suri C, McClain J, Thurston G, et al. Increased vascularization in mice overexpressing angiopoietin-1. *Science*. 1998;282(5388):468–471.
11. Thurston G, Suri C, Smith K, et al. Leakage-resistant blood vessels in mice transgenically overexpressing angiopoietin-1. *Science*. 1999;286(5449):2511–2514.
12. Winkler F, Kozin SV, Tong RT, et al. Kinetics of vascular normalization by VEGFR2 blockade governs brain tumor response to radiation: role of oxygenation, angiopoietin-1, and matrix metalloproteinases. *Cancer Cell*. 2004;6(6):553–563.
13. Chae SS, Kamoun WS, Farrar CT, et al. Angiopoietin-2 interferes with anti-VEGFR2-induced vessel normalization and survival benefit in mice bearing gliomas. *Clin Cancer Res*. 2010;16(14):3618–3627.
14. Holopainen T, Saharinen P, D'Amico G, et al. Effects of angiopoietin-2-blocking antibody on endothelial cell-cell junctions and lung metastasis. *J Natl Cancer Inst*. 2012;104(6):461–475.
15. Koh YJ, Kim HZ, Hwang SI, et al. Double antiangiogenic protein, DAAP, targeting VEGF-A and angiopoietins in tumor angiogenesis, metastasis, and vascular leakage. *Cancer Cell*. 2010;18(2):171–184.
16. Mazzieri R, Pucci F, Moi D, et al. Targeting the ANG2/TIE2 axis inhibits tumor growth and metastasis by impairing angiogenesis and disabling rebounds of proangiogenic myeloid cells. *Cancer Cell*. 2011;19(4):512–526.
17. Leow CC, Coffman K, Inigo I, et al. MEDI3617, a human anti-angiopoietin 2 monoclonal antibody, inhibits angiogenesis and tumor growth in human tumor xenograft models. *Int J Oncol*. 2012;40(5):1321–1330.
18. Huang H, Lai JY, Do J, et al. Specifically targeting angiopoietin-2 inhibits angiogenesis, Tie2-expressing monocyte infiltration, and tumor growth. *Clin Cancer Res*. 2011;17(5):1001–1011.
19. Jain RK, Carmeliet P. SnapShot: tumor angiogenesis. *Cell*. 2012;149(6):1408–1408 e1.
20. Winderlich M, Keller L, Cagna G, et al. VE-PTP controls blood vessel development by balancing Tie-2 activity. *J Cell Biol*. 2009;185(4):657–671.
21. Amarasinghe KK, Evdokimov AG, Xu K, et al. Design and synthesis of potent, non-peptidic inhibitors of HPTPbeta. *Bioorg Med Chem Lett*. 2006;16(16):4252–4256.
22. Nicoli S, Presta M. The zebrafish/tumor xenograft angiogenesis assay. *Nat Protoc*. 2007;2(11):2918–2923.
23. Kojima H, Sakurai K, Kikuchi K, et al. Development of a fluorescent indicator for nitric oxide based on the fluorescein chromophore. *Chem Pharm Bull (Tokyo)*. 1998;46(2):373–375.
24. Nottebaum AF, Cagna G, Winderlich M, et al. VE-PTP maintains the endothelial barrier via plakoglobin and becomes dissociated from VE-cadherin by leukocytes and by VEGF. *J Exp Med*. 2008;205(12):2929–2945.
25. Baumer S, Keller L, Holtmann A, et al. Vascular endothelial cell-specific phosphotyrosine phosphatase (VE-PTP) activity is required for blood vessel development. *Blood*. 2006;107(12):4754–4762.
26. Dominguez MG, Hughes VC, Pan L, et al. Vascular endothelial tyrosine phosphatase (VE-PTP)-null mice undergo vasculogenesis but die embryonically because of defects in angiogenesis. *Proc Natl Acad Sci U S A*. 2007;104(9):3243–3248.
27. Li Z, Huang H, Boland P, et al. Embryonic stem cell tumor model reveals role of vascular endothelial receptor tyrosine phosphatase in regulating Tie2 pathway in tumor angiogenesis. *Proc Natl Acad Sci U S A*. 2009;106(52):22399–22404.
28. Vakoc BJ, Lanning RM, Tyrrell JA, et al. Three-dimensional microscopy of the tumor microenvironment in vivo using optical frequency domain imaging. *Nat Med*. 2009;15(10):1219–1223.
29. Kashiwagi S, Izumi Y, Gohongi T, et al. NO mediates mural cell recruitment and vessel morphogenesis in murine melanomas and tissue-engineered blood vessels. *J Clin Invest*. 2005;115(7):1816–1827.
30. Kashiwagi S, Tsukada K, Xu L, et al. Perivascular nitric oxide gradients normalize tumor vasculature. *Nat Med*. 2008;14(3):255–257.
31. Sfiligoi C, de Luca A, Cascone I, et al. Angiopoietin-2 expression in breast cancer correlates with lymph node invasion and short survival. *Int J Cancer*. 2003;103(4):466–474.
32. Nasarre P, Thomas M, Kruse K, et al. Host-derived angiopoietin-2 affects early stages of tumor development and vessel maturation but is dispensable for later stages of tumor growth. *Cancer Res*. 2009;69(4):1324–1333.
33. Kienast Y, von Baumgarten L, Fuhrmann M, et al. Real-time imaging reveals the single steps of brain metastasis formation. *Nat Med*. 2010;16(1):116–122.
34. Weis S, Cui J, Barnes L, Cheresh D. Endothelial barrier disruption by VEGF-mediated Src activity potentiates tumor cell extravasation and metastasis. *J Cell Biol*. 2004;167(2):223–229.
35. O'Reilly MS, Holmgren L, Shing Y, et al. Angiostatin: a novel angiogenesis inhibitor that mediates the suppression of metastases by a Lewis lung carcinoma. *Cell*. 1994;79(2):315–328.
36. Sorensen AG, Emblem KE, Polaskova P, et al. Increased survival of glioblastoma patients who respond to antiangiogenic therapy with elevated blood perfusion. *Cancer Res*. 2012;72(2):402–407.
37. Wilson WR, Hay MP. Targeting hypoxia in cancer therapy. *Nat Rev Cancer*. 2011;11(6):393–410.

38. Hamzah J, Jugold M, Kiessling F, et al. Vascular normalization in Rgs5-deficient tumours promotes immune destruction. *Nature*. 2008;453(7193):410–414.
39. Johansson A, Hamzah J, Payne CJ, Ganss R. Tumor-targeted TNFalpha stabilizes tumor vessels and enhances active immunotherapy. *Proc Natl Acad Sci U S A*. 2012;109(20):7841–7846.
40. Oubaha M, Gratton JP. Phosphorylation of endothelial nitric oxide synthase by atypical PKC zeta contributes to angiopoietin-1-dependent inhibition of VEGF-induced endothelial permeability in vitro. *Blood*. 2009;114(15):3343–3351.
41. Aerpio. Aerpio announces positive phase 1 data on first-in-class Tie-2 activator, AKB-9778, in development for diabetic macular edema. *2012*. http://www.aerpio.com/news/Aerpio-Phase-1-9778.pdf. Accessed June 16, 2013.

Funding

The work was supported in part by the US Department of Defense Breast Cancer Research Innovator Award W81XWH-10-1-0016 (RKJ); US National Cancer Institute grants R01-CA126642 (RKJ), P01-CA080124 (RKJ, DF, and DGD), R01-CA096915 and S10-RR027070 (DF), R01-CA159258 (DGD), R01-CA163528 (BJV), T32-CA073479 (CTK), and R00-CA137167 (TPP); National Institutes of Health DP2OD008780 (TPP); NCI/Federal Share Proton Beam Program Income (RKJ, TPP, and DGD); and American Cancer Society grant RSG-11-073-01TBG (DGD). SG has been supported by fellowships from the Australian-American Fulbright Commission, the American Society of Clinical Oncology, and the Australian-American Association. NG has received fellowships from Dittmer Fonds, the Dutch Cancer Society, Vrije Universiteit (all Amsterdam, Netherlands) and Stichting Bekker-la Bastide-Fonds (Rotterdam, Netherlands). YH is supported by DoD Research Fellowship W81XWH-11-1-0619. MS is the recipient of a Paul Calabresi Career Development Award in Clinical Oncology (2K12CA090354-11) at the Massachusetts General Hospital. This project was also supported by the Center for Biomedical OCT Research and Translation through grant P41EB015903, awarded by the National Center for Research Resources and the National Institute of Biomedical Imaging and Bioengineering of the National Institutes of Health.

Notes

R.K. Jain received research grants from Dyax, MedImmune, and Roche; received consultant fees from Dyax, Enlight, Noxxon, and SynDevRx; owns equity in Enlight, SynDevRx, and XTuit; and serves on the Board of Directors of XTuit and Boards of Trustees of H&Q Healthcare Investors and H&Q Life Sciences Investors. No reagents or funds from these organizations were used in this study. All other authors declare no conflicts. The funders of the study had no role in the design of the study; the collection, analysis, and interpretation of the data; the writing of the manuscript; and the decision to submit the manuscript for publication.

The authors thank Carolyn Smith, Eve Smith, Sylvie Roberge, and Julia Kahn for their expert technical assistance and Peigen Huang for help with animal studies. We thank Akebia Therapeutics for providing AKB-9778, and Dr Brett Bouma for his assistance with optical frequency domain imaging.

Affiliations of authors: Edwin L. Steele Laboratory for Tumor Biology, Department of Radiation Oncology (SG, NG, MS, CTK, NDK, TH, YH, JDM, EA, RS, TPP, DGD, DF, RKJ) and Wellman Center for Photomedicine (BJV), Massachusetts General Hospital and Harvard Medical School, Boston, MA; Cardiovascular Research Center, Massachusetts General Hospital and Harvard Medical School, Charlestown, MA (BPW, RTP); Current affiliation: Department of Pathology, NYU Langone Medical Center and School of Medicine, New York, NY (MS); Department of Biology (SW) and Department of Chemical Engineering (JY), Massachusetts Institute of Technology, Cambridge.